The Effect of Thermal Cycling on Steam Oxidation Behaviour of TP347H FG at 650°C

Mobbs, Rebecca-Louise; Osgerby, Steve; Taylor, Mary; Evans, Hugh

DOI:
10.1080/09603409.2017.1389380

Materials at High Temperatures

The Effect of Thermal Cycling on Steam Oxidation Behaviour of TP347H FG at 650 °C

--Manuscript Draft--

Manuscript Number:	MHT595
Full Title:	The Effect of Thermal Cycling on Steam Oxidation Behaviour of TP347H FG at 650 °C
Article Type:	Special Issue Article
Keywords:	Steam oxidation; Spallation; TP347H FG; Austenitic Stainless Steel
Corresponding Author:	Mary Taylor University of Birmingham UNITED KINGDOM
Corresponding Author Secondary Information:	
Corresponding Author's Institution:	University of Birmingham
Corresponding Author's Secondary Institution:	
First Author:	Rebecca-Louise Mobbs, M.Sci.
First Author Secondary Information:	
Order of Authors:	Rebecca-Louise Mobbs, M.Sci.
	Mary Taylor
	Hugh Evans, PhD
	Steve Osgerby, PhD
Order of Authors Secondary Information:	
Abstract:	The cyclic oxidation behaviour of fine-grained Type 347 stainless steel (TP347H FG) at 650 °C in air saturated steam and deoxygenated steam environments for 100-1000 hours has been investigated. Electron microscopy, energy dispersive and wavelength dispersive X-ray Spectroscopy (EDS and WDS, respectively) have been used to characterise the samples. Short term oxidation tests have shown only haematite spallation occurs whereas longer term tests have shown magnetite also spalls on cooling to room temperature. In all cases cyclic oxidation showed spallation does not occur after long term tests and is only visible in small amounts after short term tests subsequent to the initial spallation event.
Additional Information:	
Question	**Response**
Funding Information:	

The Effect of Thermal Cycling on Steam Oxidation Behaviour of TP347H FG at 650 °C

R-L. Mobbs[a], S. Osgerby[b], M. P. Taylor[a*], H. E. Evans[a]

[a]*The University of Birmingham, Birmingham, B15 2TT, UK*

[b]*GE Power, Rugby, CV21 2NH, UK*

[*]E-mail: m.p.taylor@bham.ac.uk

The Effect of Thermal Cycling on Steam Oxidation Behaviour of TP347H FG at 650 °C

The cyclic oxidation behaviour of fine-grained Type 347 stainless steel (TP347H FG) at 650 °C in air saturated steam and deoxygenated steam environments for 100-1000 hours has been investigated. Electron microscopy, Energy Dispersive and Wavelength Dispersive X-ray Spectroscopy (EDS and WDS, respectively) have been used to characterise the samples. Short term oxidation tests have shown only haematite spallation occurs whereas longer term tests have shown magnetite also spalls on cooling to room temperature. In all cases cyclic oxidation showed spallation does not occur after long term tests and is only visible in small amounts after short term tests subsequent to the initial spallation event.

Keywords: Steam oxidation; Spallation; TP347H FG; Austenitic Stainless Steel.

Introduction

The continued desire for a greener energy mix has resulted in an increased use of biomass for power generation. Although operating conditions are currently envisaged to be base load it is thought that biomass power plants may be used as peaking power plants. These will meet increases in customer demand and as such will have a more cyclic nature [1] and will be designed to operate from half load to full load conditions [2]. The impact of this cyclical behaviour on materials degradation is yet to be fully understood. One of the main factors affecting the lifetime of materials is their resistance to high temperature oxidation [3-5]. A chromium rich oxide, usually chromia, is required to protect the alloy from further oxidation [6]. During oxidation in steam conditions, such as those seen in plant, the chromium rich layer may sometimes not be continuous and as a result, iron rich oxides such as haematite and magnetite may grow, as well as $(Fe_x,Cr_{1-x})_3O_4$ spinels. When the biomass power plants undergo thermal cycling the non-protective iron rich oxides may spall as a result in a mismatch

of thermal expansion coefficients between the alloy and oxide [7]. The spallation of oxides grown at high temperature can cause tube blockages and can induce unexpected shutdowns [8, 9]. When plant restart occurs, the non-protective spinel oxide that has remained adherent, or in some cases the bare metal, will be exposed to the oxidising gas and may result in rapid oxidation of the chromium depleted alloy [10].

Current coal fired plants that are being converted to biomass fired plants use TP347H FG, an austenitic stainless steel, in the superheater and reheater boiler tubing, where TP is tube piping, H is high carbon content and FG is fine-grained. Previous studies [11] that have exposed this steel to pressurised (25 MPa) steam between 499 and 650 °C and oxidised for times up to 57554 hours found that a duplex scale consisting of an outer iron rich oxide and an inner Fe-Cr-Ni spinel developed. It has also been found that between 500 and 800 °C TP347H FG forms a duplex scale when exposed to steam [12]. The outer iron rich oxide has been found to be a mixture of haematite and magnetite [6, 13].

Experimental Procedure

Cyclic oxidation in air saturated and deoxygenated steam was carried out at atmospheric pressure on TP347H FG austenitic stainless steel, the composition of which is shown in Table 1.

Table 1. Nominal composition of TP347H FG provided by the data sheet supplied.

	C	Si	Mn	S	P	Ni	Cr	Nb	Fe
wt.%	0.09	0.4	1.48	0.001	0.026	11.34	18.21	0.88	Balance
at.%	0.41	0.79	1.49	0.002	0.046	10.66	19.32	0.52	Balance

Samples were extracted from standard tubes, as used in plant, with a pickled inner surface. The tube had an internal diameter of 28 mm and a wall thickness of 4.5 mm. A silicon carbide disc was used to cut the tubing into 10 mm slices and these

sections were subsequently cut into approximately 60° arcs producing 6 samples from each 10 mm section. All samples were cleaned in ethanol prior to exposure in the custom made rigs, Figure 1.

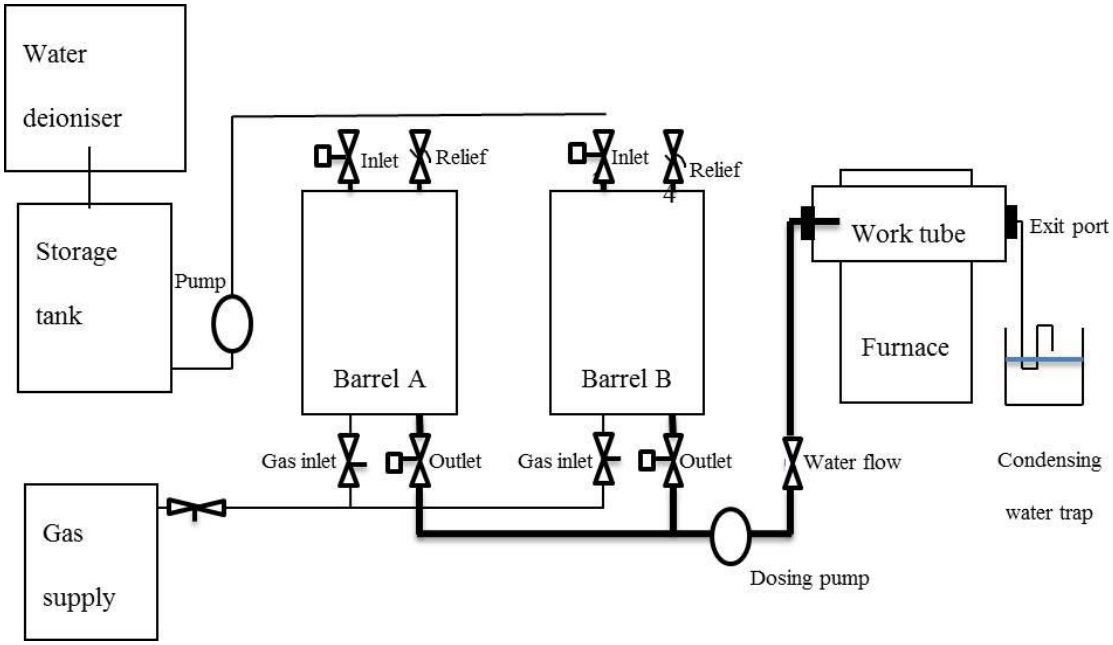

Figure 1. Schematic diagram of the steam oxidation set up.

Deionised water was supplied to two water barrels, A and B, via a pump. The water barrels were pressurised to approximately 0.5 bar using either air or nitrogen to achieve the air saturated or deoxygenated steam environments, respectively. A Hach Orbisphere 410 oxygen meter was used to measure the oxygen partial pressure. When using a deoxygenated environment the water was degassed for 24 hours prior to use. A dosing pump transfers the water from the barrels to the worktube where it evaporates on entry and travels to the exit port where it is condensed. This ensured the steam flow was unidirectional. The capacity of the water tanks was monitored during testing by weighing scales. The design of the rig was such that the barrels could be filled and emptied independently ensuring continuous flow during long term testing. In all cases the steam flow was set up and was monitored to ensure stable behaviour and flow had

been achieved prior to inserting the samples through the exit port. At the end of the test period samples were removed and cooled in laboratory air.

Previous experience with this rig has shown that under laboratory conditions, the air saturated steam environment generated in the rig produced oxide compositions and morphologies that replicate those seen in plant conditions for longer times, despite the fact deoxygenated steam is more representative of plant. Previous research has also shown that spallation does not occur under deoxygenated conditions, so air saturated steam has mainly been used in the current work to initiate spallation after the first thermal exposure [14]. Details of the testing performed are given in Table 2. A 300 hour thermal cycle (three 100 hour exposures) was performed and compared to a 300 hour isothermal test. The 1000 hour thermal cycles include both air saturated and deoxygenated steam environments. A comparison will be drawn between these two different environments and also to the 100 hour thermal cycles. All tests were performed at 650 °C.

Spalled oxide was collected for examination in a scanning electron microscope (SEM). After each cycle the surface of samples were examined in a JEOL 6060 SEM. A thin cross section was removed and prepared for analysis. For thermal cycling, samples were returned to the furnace for further testing.

For cross sectional analysis, samples were mounted in epoxy resin, ground using progressively finer SiC papers from 240 to 1200 grit. This was followed by polishing using diamond paste and finished using an OPA-sol. A JEOL 7000 FEG SEM with Energy Dispersive X-ray Spectroscopy and Wavelength Dispersive X-ray Spectroscopy (EDS/ WDS) capabilities was used to examine the oxide on the inner, pickled surface, i.e. steam side, of the tubing in plant. Oxide thicknesses were measured in order to determine oxidation kinetics where 100 measurements were taken at equal spacings for

each sample. In the case of the Fe-Cr-Ni spinel a systematic error is included since the oxide is thinner nearer the grain boundaries. Spallation of the outer iron rich oxides causes difficulties in data interpretation, so oxide growth kinetics for magnetite and haematite have not been included here.

Between 15 and 30 EDS/ WDS measurements were taken to obtain average oxide composition values.

Results

The oxide spallation behaviour for each test is presented in Table 2. Estimates of the spalled area fraction obtained from SEM images of the inner pickled surface shows that significant spallation occurred after the first thermal cycle in all series, Figure 2.

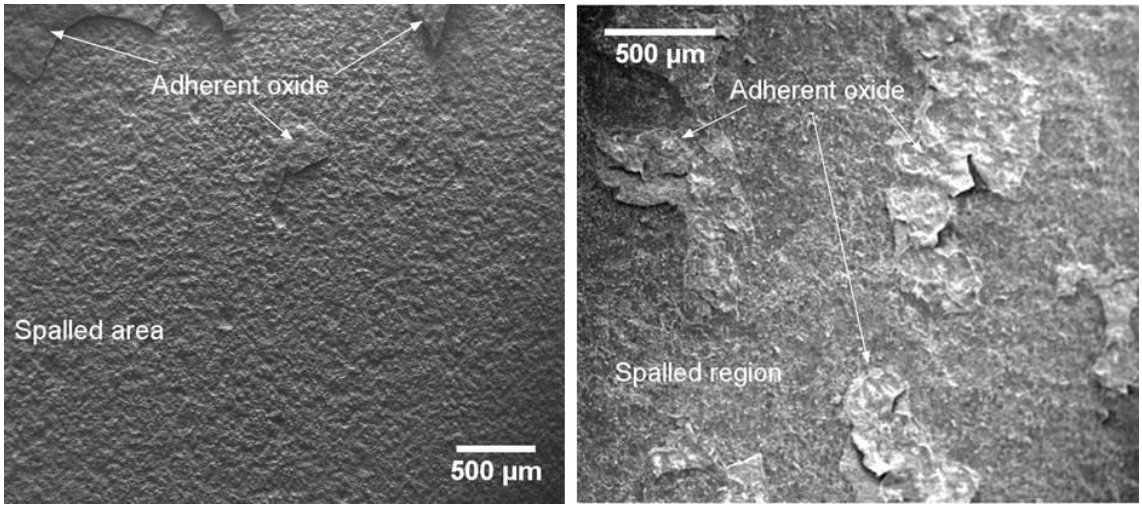

Figure 2. Secondary electron images of the inner pickled surface of TP347H FG exposed to air saturated steam at 650 °C for 100 hours (left) and 1000 hours (right).

Table 2. Details of the test matrix and spallation observations of TP347H FG after cooling in laboratory air to room temperature.

Cycle	Total Exposure	Steam Conditions	Observations	Area fraction of spallation (%)
1) 100 hours	300 hours	Air saturated steam, 650 °C	Fe_2O_3 spalled	80.8
2) 100 hours			Fe_3O_4 spalled	15.7
3) 100 hours			No visible spallation	0.0
1) 300 hours	300 hours	Air saturated steam, 650 °C	Fe_2O_3 + Fe_3O_4 spalled	74.5
1) 1000 hours	2000 hours	Air saturated steam, 650 °C	Fe_2O_3 + Fe_3O_4 spalled	70.9
2) 1000 hours			No visible spallation	0.0
1) 1000 hours	2000 hours	Air saturated steam, 650 °C	Fe_2O_3 + Fe_3O_4 spalled	50.2
2) 1000 hours		Deoxygenated steam, 650 °C	No visible spallation	0.0

An optical image of a cross section of the sample exposed for 1000 hours, Figure 3, shows the expected formation of a duplex oxide scale consisting of an inwardly growing Fe-Cr-Ni spinel and the outwardly growing iron rich oxides. This is similar to what has been reported in the literature [6, 11-13]. Optical microscopy reveals a difference in contrast between haematite and magnetite that is not seen under SEM. Haematite appears a marginally darker grey than magnetite under optical conditions, Figure 3. The composition of the two different oxide layers has been

confirmed using WDS analysis of polished cross sections of unspalled regions of TP347H FG, Figure 4.

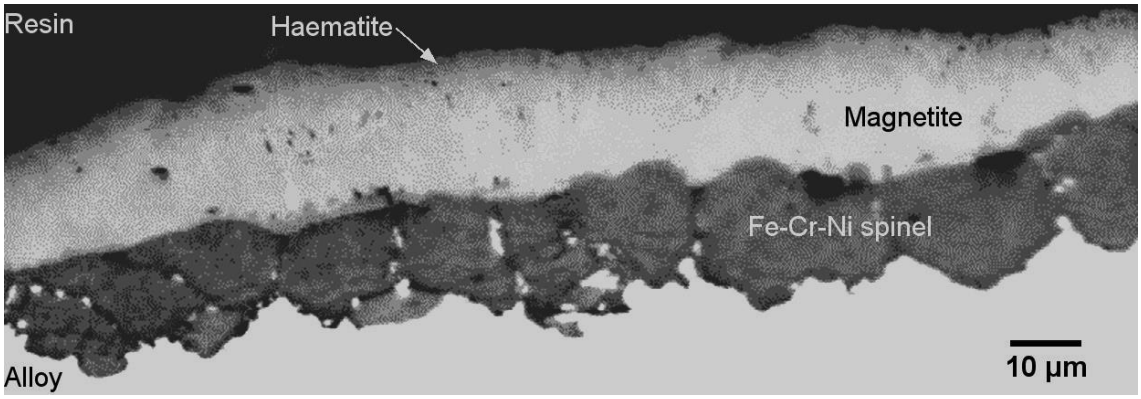

Figure 3. Optical microscope image of a cross section through an unspalled region of TP347H FG exposed to air saturated steam for 1000 hours at 650 °C showing two outer iron rich oxides.

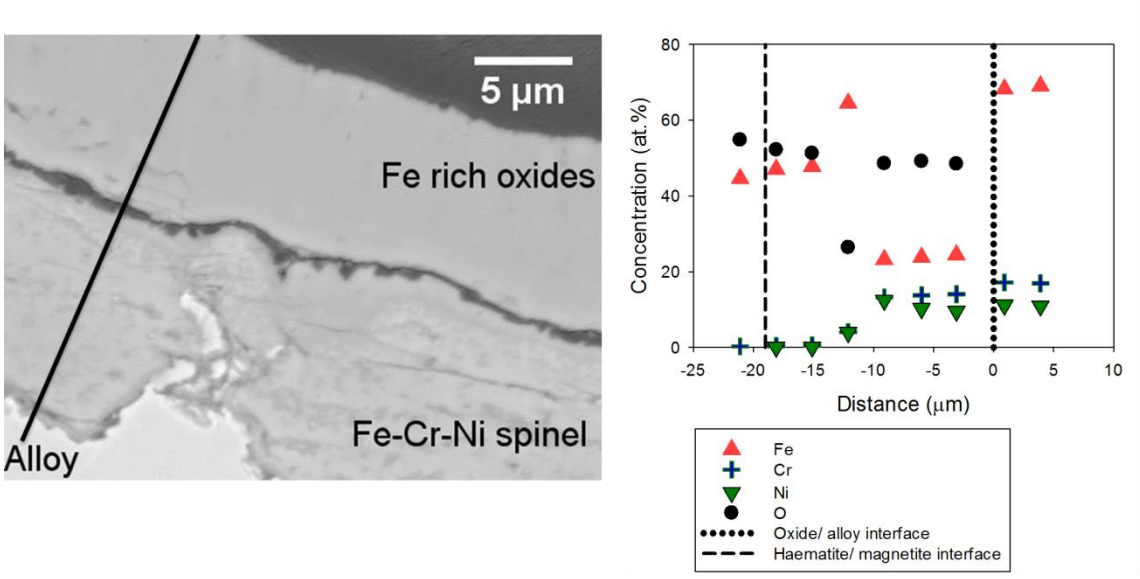

Figure 4. Back scattered electron cross section image through TP347H FG oxidised in air saturated steam for 1 x 100 hours at 650 °C (left) and the corresponding concentration profile measured using EDS and WDS showing the presence of Fe_2O_3 (40 at.% Fe, 60 at.% O) and Fe_3O_4 (42.9 at.% Fe, 57.1 at.% O) (right).

After the first 100 hours steam oxidation exposure, only haematite spalled. For longer exposure times, 1000 hours, images of the spalled particles indicate two distinguishable oxide morphologies suggesting that both haematite and magnetite

spalled at longer times. The magnetite was composed of plate like grains of high aspect ratio oriented approximately parallel to the oxide growth direction. The haematite was composed of much smaller equiaxed grains. In some cases there appears to be a very clear boundary between the two oxide layers. A crack at the magnetite/ spinel interface has confirmed that spallation occurred along that interface, Figure 5. This crack has been suggested to occur as a result of void formation. These are visible where the crack broadens and so must have been present prior to crack formation. Magnetite grows by cation diffusion where haematite grows by anion diffusion [15] and voids form as a result of the rapid diffusion of metal ions through the scale [16]. These voids therefore appear at the magnetite/ spinel interface causing a plane of weakness.

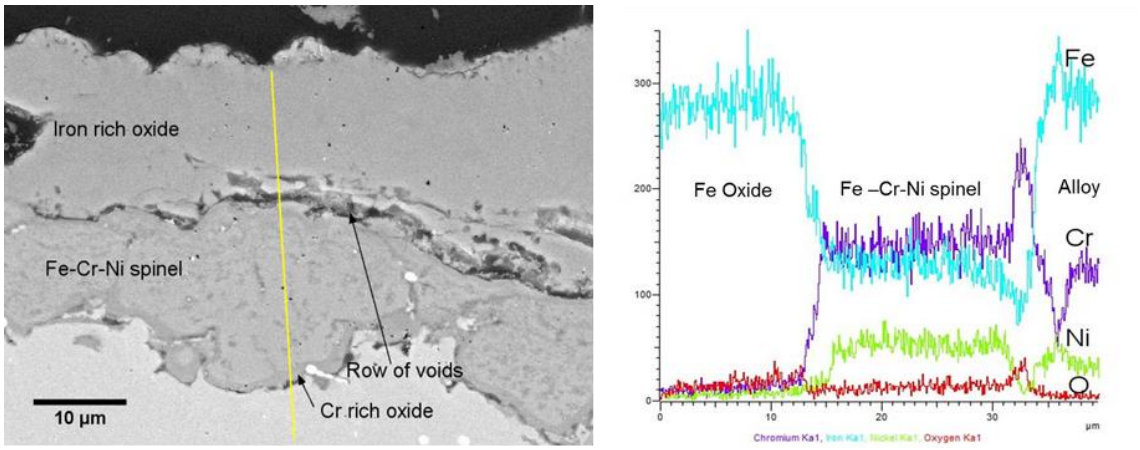

Figure 5. Back scattered electron cross section image of TP347H FG oxidised in air saturated steam for 1 x 300 hours at 650 °C (left) and the corresponding linescan profile measured along the yellow line using EDS, demonstrating the chromium rich oxide and the depletion seen beneath this layer (right).

The amount of visible spallation decreased after the second 100 hour thermal cycle and there was no visible spallation after the third thermal cycle, Table 2. There were similar findings for the 1000 hour tests where no further spallation occurred in subsequent thermal cycles. EDS and oxide morphologies indicate that no haematite regrowth occurred after the initial spallation event. This suggests that spallation will only occur whilst there is adherent haematite. Clearly the haematite/ magnetite

interface is more strongly bonded and so spallation occurs at the weakest interface, i.e. at the voids. The change in steam environment for the second cycle also had no effect on this.

Table 3 details the concentration of iron observed within the spinel from WDS/ EDS cross sectional analysis and the average thicknesses measured for each oxide layer. The 100 hour tests resulted in an increase in the average spinel thickness and an increase in the average iron concentration from 15-30 EDS/ WDS readings. Cross sections from these tests show the iron rich oxide begins to reform during the third thermal cycle.

EDS and WDS analysis showed that the Fe concentration within the spinel oxide after 300 hours of isothermal exposure was 26.3 at.% which is slightly less than that seen after 300 hours of thermal cycling, 33.0 at.%. The thickness of the spinel oxide after the isothermal exposure is also slightly less at 12.5 μm compared to 16.4 μm for the thermally cycled sample.

The average spinel oxide thickness and the average concentration of iron within this layer is shown to decrease with 1000 hour thermal cycling. An iron rich oxide is shown to regrow during the second thermal cycle under both environmental conditions tested but is thicker under deoxygenated conditions compared to air saturated steam. The iron rich oxide formed during the second thermal cycle was found to be magnetite and there was no evidence of haematite growth.

Table 3. Cross section oxide thickness data and iron concentrations of TP347H FG after oxidation in steam at 650 °C for different durations.

Oxidation time (hours)	Average Fe concentration in spinel (at.%) measured from EDS	Average spinel thickness (μm)	Maximum spinel thickness (μm)	Average Fe oxide thickness (μm)	Average Cr oxide thickness (μm)
1 x 100	23.0	9.7±3.6	20.4	3.2±1.2	
2 x 100	30.5	13.1±5.1	21.9	0.0	
3 x 100	33.9	16.4±5.9	27.3	5.4±2.4	
1 x 300	26.3	12.5±6.3	35.2	15.6±3.0	1.2±0.6
1 x 1000	28.6	18.4±9.1	31.6	0.0	1.5±1.0
2 x 1000	24.8	15.2±4.3	22.1	7.9±1.3	2.5±1.2
1 x 1000	24.7	15.2±5.3	29.5	0.0	1.5±0.8
2 x 1000	19.2	13.5±6.4	27.1	14.0±5.6	1.7±0.9

In addition, a chromium rich oxide begins to grow at the base of the spinel but is not continuous until an isothermal exposure of 300 hours, Figure 5 (left). Where the chromium rich oxide forms, a depletion of chromium occurs up to 5 μm into the alloy, Figure 5 (right). The concentration profile shown in Figure 6 demonstrates the presence of the chromium rich oxide. Small amounts of iron were also detected within this region as a result of the interaction volume of the EDS/ WDS detectors and as such there will be some interference from the Fe-Cr-Ni spinel and the alloy. TEM analysis would confirm the composition of the chromium rich oxide however it is not within the scope of the current work.

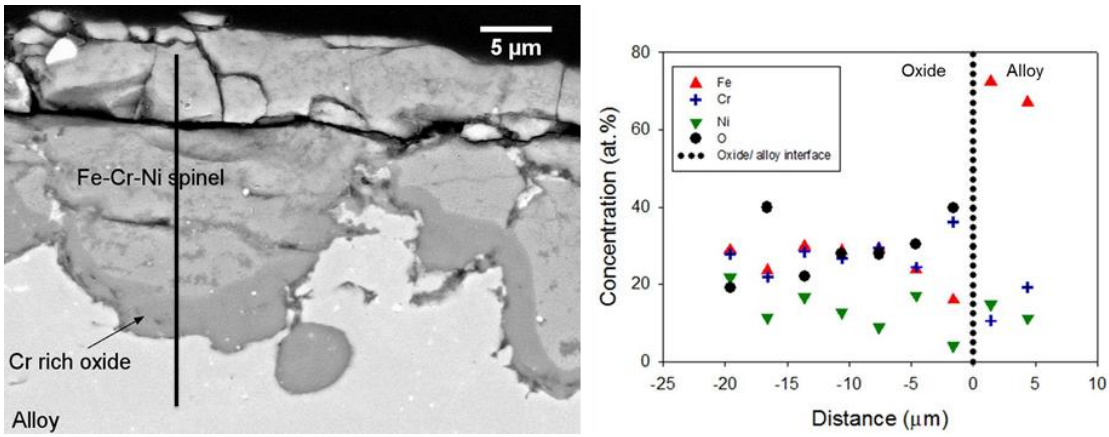

Figure 6. BSE cross section image of TP347H FG oxidised in air saturated steam for 1 x 1000 hours at 650 °C (left) and the corresponding concentration profile measured using EDS and WDS showing the chromium rich oxide layer (right).

For the 2000 hour thermal cycling tests, the chromium rich oxide is seen to continue growing. The extent of growth differs depending on the steam environment, Table 3, with the thickness increasing to a greater extent under air saturated steam. EDS/ WDS analysis was performed on these samples, Figure 7, and shows that the depth of depletion of chromium is greater under air saturated steam compared to deoxygenated steam. This confirms that a thicker oxide has grown under air saturated conditions.

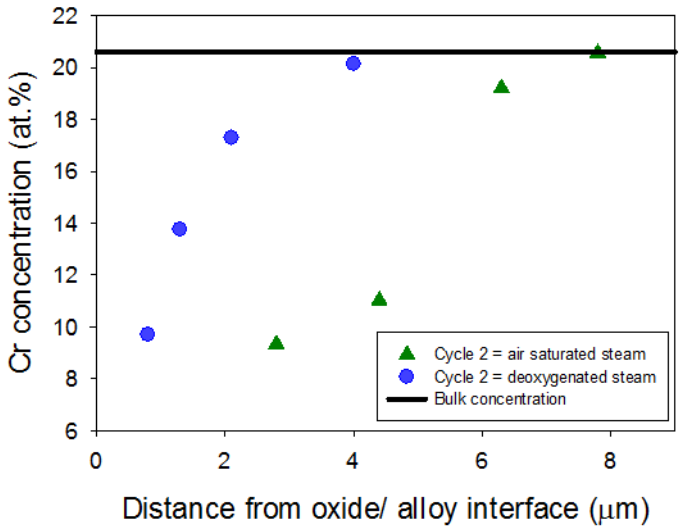

Figure 7. Depletion profiles measured using EDS of TP347H FG oxidised in steam for a total of 2000 hours at 650 °C where the second 1000 hours was carried out in a different environment. A greater depth of depletion was observed when oxidation was performed in air saturated steam.

Oxidation Kinetics

Oxide thickness measurements have been used to calculate rate constants of the spinel for both isothermal and cyclic exposures.

A plot of oxide thickness as a function of oxidation time, Figure 8, has been used to calculate the rate constant, n, for both isothermal and cyclic conditions as per the following equation:

$$\xi = (k_n t)^{1/n} \quad (1)$$

where ξ is oxide thickness, k_n is the rate constant and t is time.

The value of n, determined from a log log plot of Equation 1, was calculated to be 2.9 and 2.0 showing sub parabolic and parabolic kinetics for isothermal and cyclic exposures, respectively. Values for the rate constant, k_n, were calculated to be 1.3×10^{-15} and 3.6×10^{-15} m^2 s^{-1} for isothermal and cyclic exposures, respectively.

The cyclic oxidation kinetics follow parabolic behaviour. However, the isothermal data shows cubic kinetics, leading to thinner than expected spinel thickness at times >100 hours if based on parabolic kinetics. It is postulated that this is due to the formation of the chromium rich layer at the spinel/ alloy interface which was observed to be continuous at approximately 300 hours. Once fully formed, this will dominate the oxidation kinetics for the whole system and reduce oxidation rates.

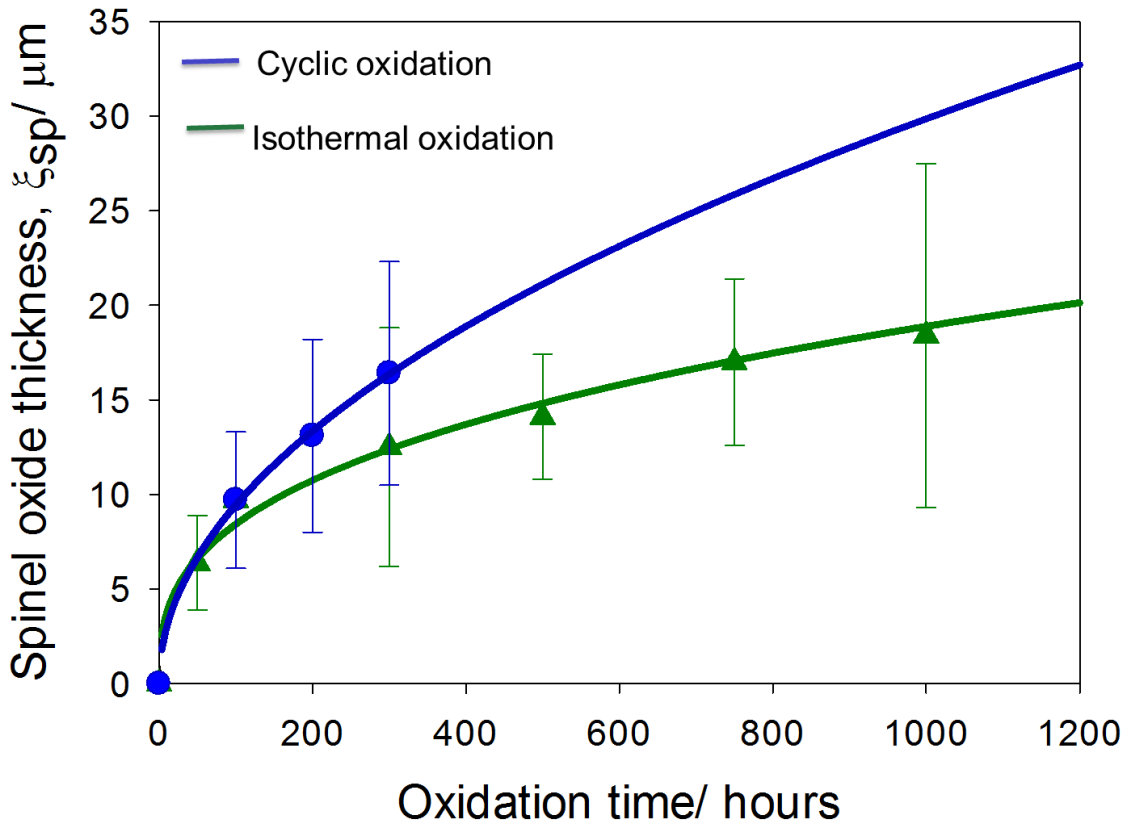

Figure 8. Oxidation kinetics for both isothermal (triangles) and cyclic (circles) oxidation for TP347H FG exposed to air saturated steam at 650 °C.

The parabolic rate constants were found to be two orders of magnitude higher than the k_p values stated in the literature, 1.7 x 10^{-17} m^2 s^{-1} [13], however it has been noted that oxidation kinetics do tend to be higher for shorter term tests [17]. This literature value is also for the total oxide thickness for TP347H FG from plant trials where the steam environment will be slightly different from those in this study. Rosser *et al.* [14] found the parabolic rate constant for spinel on shot peened Super 304 H, with similar composition to TP347H FG, in deoxygenated steam to be 1.9 x 10^{-16} m^2 s^{-1}. This is closer in agreement to the results found in this study and is a more appropriate comparison. The absence of available kinetic data for spinel growth in the literature precludes a wider comparison.

Discussion

In all cases, the first exposure results in the formation of an outer layer of haematite, which, on cooling, undergoes substantial spallation. Haematite formation has been found to favour spallation due to the mismatch of the thermal expansion coefficients between oxide and alloy [13] which is part of a larger study. However, re-exposure does not lead to further formation of haematite with a noticeable reduction in spallation.

Under short term cyclic conditions loss of the iron rich magnetite oxide continues to occur on cooling. Simultaneously, a protective chromium rich layer develops at the base of the spinel but is not continuous until 300 hours. The Fe concentration within the spinel increases during this time. It is postulated that the formation of the chromium rich oxide leads to a decrease in the amount of chromium diffusion into the spinel, hence increasing the iron concentration. It is also postulated that the greater spinel thickness seen in thermal cycling compared to isothermal exposures for 300 hours is as a result of iron oxide spallation. Haematite spalls on cooling after the first thermal cycle, so the oxygen diffusing inwardly to form the spinel oxide has a reduced area to diffuse through whereas for the case of isothermal exposure where the iron rich oxide is adherent, the diffusion of oxygen will be reduced and therefore the spinel cannot grow to the same extent.

However, for longer thermal cycles, the reverse was observed, i.e. the iron concentration within the spinel and the spinel thickness reduced. Under these conditions, the chromium rich layer had become continuous prior to the initial spallation event. Table 4 gives details of the bulk, D_b, and in some cases grain boundary, D_{gb}, diffusion coefficients of chromium, iron and oxygen in austenitic stainless steel as well as through different oxides. The diffusion of iron through thin films of chromia is two orders of magnitude slower compared to the diffusion of iron through the alloy lattice

and four orders slower than that seen through magnetite. Since magnetite possesses an inverse spinel structure [18] it is safe to assume the diffusion coefficients of iron within the Fe-Cr-Ni spinel oxide formed on TP347H FG will be of the same order of magnitude as the self-diffusion coefficients in magnetite. Thus, on further oxidation, there is a reduced supply of iron into the spinel due to the protective nature of the chromium rich layer while the iron rich oxide continues to grow. It is postulated that this is due to iron diffusion from the spinel, Figure 9, hence the decrease in spinel oxide thickness.

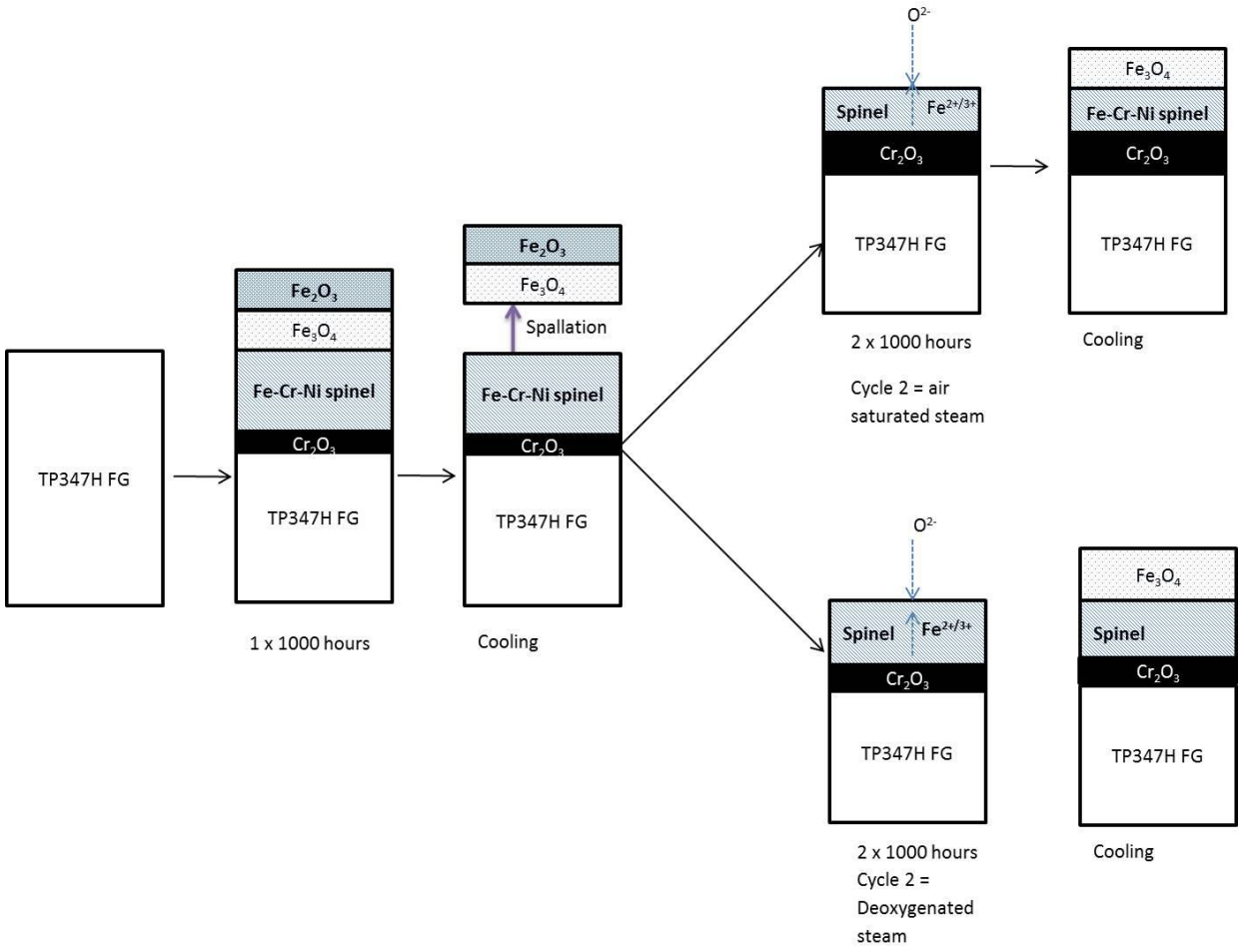

Figure 9. Oxidation mechanism for long term thermal cycling of TP347H FG.

Three interesting observations can be made between the two steam environments used for long term testing. Firstly, the growth rate of the chromium rich layer is greater under air saturated conditions than under deoxygenated environments. Secondly, in both cases, the spinel thickness reduces but to a greater extent under air saturated steam. Thirdly, the regrowth of the magnetite layer is faster under deoxygenated conditions. This is shown schematically in Figure 9. The difference in the oxygen partial pressure in the two environments must be the influencing factor.

The partial pressure of oxygen within the air saturated and deoxygenated environments have been previously measured as 1×10^{-5} and 1×10^{-8} respectively. Note that partial pressure is here defined as the ratio of oxygen pressure to the standard state of 1 atmosphere. As such, the values are dimensionless. The higher oxygen content in the air saturated steam environment means there is a larger amount of oxygen available for oxidation.

Table 4. Iron and chromium diffusion coefficients in austenitic stainless steels, chromia thin films and spinel oxides.

	T (°C)	D_{gb} ($cm^2\ s^{-1}$)	D_b ($cm^2\ s^{-1}$)
Fe in austenitic steel [19]	600		2.8×10^{-16}
Cr in austenitic steel [19]	600		1.0×10^{-16}
Fe in Cr_2O_3 [20]	740	5.9×10^{-12}	3.5×10^{-18}
Cr in Cr_2O_3 [20]	700	5.1×10^{-13}	2.9×10^{-18}
O in Fe_3O_4 [21]	650		1.0×10^{-16}
Fe in Fe_3O_4 [22]	650		3.2×10^{-14}
Fe in Fe_2O_3 [23]	650		1.6×10^{-19}

Previous studies have suggested that, with longer exposure times, the spinel oxide was thought to become more protective to oxidative attack, hence preventing any

outward iron diffusion. The magnetite layer, with no supply of iron, is then further oxidised to haematite. If this is indeed the case, the results of the current work indicate that much longer oxidation times are required for the formation of haematite [24, 25].

Conclusions

- Haematite formation has been found to be essential for spallation and as a result the amount of spallation decreases with increasing oxidation time and with each thermal cycle.
- The protective chromium rich layer is not continuous under short term testing, therefore allowing the Fe-Cr-Ni spinel to grow under thermal cycling conditions. The presence of a continuous chromium rich layer during longer term testing slows the diffusion of iron from within the alloy and so the spinel oxide is reduced in thickness.
- The diffusion of chromium to form the chromium rich oxide results in less diffusion into the spinel, therefore increasing the iron concentration.

Acknowledgements

The authors would like to thank the UK Engineering and Physical Science Research Council (EPSRC) and BF2RA for financial support for this work. Funding for this work is also provided as part of the Efficient Fossil Energy Technologies (EFET) doctorate centre. The authors would also like to thank the centre for electron microscopy (CEM) at the University of Birmingham for technical support with SEMs.

References:

[1]Calmunger M. On High-Temperature Behaviours of Heat Resistant Austenitic Alloys [dissertation]. Linkoping, Linkoping University, 2015.

[2]Srinivas T, Reddy BV. Hybrid Solar-Biomass Power Plant Without Energy Storage. Case Studies in Thermal Engineering. 2014; 2: 75-81.

[3]Fry AT, Osgerby S, Wright M. Oxidation of Alloys in Steam Environments – A Review: NPL; 2002 (Report MATC(A)).

[4]Dudziak T, Lukaszewicz M, Simms N, Nicholls J. Analysis of High Temperature Steam Oxidation of Superheater Steels Used in Coal Fired Boiler. Oxid. Met. 2016; 85(1-2): 171-187.

[5]Schutze M. Shrier's Corrosion. Oxford: Elservier; 2010. 1.08, Stress Effects in High Temperature Oxidation of Metals; p.153-179.

[6]Wright IG, Dooley RB. A Review of the Oxidation Behaviour of Structural Alloys in Steam. Int. Mater. Rev. 2010; 55: 129-167.

[7]Robertson J, Manning MI. Limits to Adherence of Oxide Scales. Mater. Sci. Technol. 1990; 6: 81-91.

[8]Pantleon K, Montgomery M. Phase Identification and Internal Stress Analysis of Steamside Oxides on Plant Exposed Superheater Tubes. Metall. Mater. Trans. A. 2012; 43(5): 1477-1486.

[9]Ennis P, Quadakkers W. Implications of Steam Oxidation for the Service Life of High-Strength Martensitic Steel Components in High-Temperature Plant. Int. J. Press. Vessels Pip. 2007; 84: 82-87.

[10]Evans HE, Mitchell GP, Lobb RC, Owen DR. A Numerical Analysis of Oxide Spallation. Proceedings: Mathematical and Physical Sciences. 1993; 440(1908): 1-22.

[11]Hansson AN, Danielsen H, Grumsen FB, Montgomery M. Microstructural Investigation of the Oxide Formed on TP347H FG During Long-Term Steam Oxidation. Mater. Corros. 2010; 61(8): 665-675.

[12]Hansson AN, Pantleon K, Grumsen FB, Somers MA. Microstructure Evolution During Steam Oxidation of a Nb Stabilised Austenitic Stainless Steel. Oxid. Met. 2010; 73: 289-309.

[13]Wright IG, Dooley RB. Morphologies of Oxide Growth and Exfoliation in Superheater and Reheater Tubing of Steam Boilers. Mater. High. Temp. 2011; 28(1): 40-57.

[14]Rosser JC, Bass MI, Cooper C, Lant T, Brown PD, Connolly BJ, Evans HE. Steam Oxidation of Super 304H and Shot-peened Super 304H. Mater. High. Temp. 2012; 29(2): 95-106.

[15]Caplan D, Cohen M. Scaling of Iron at 500 °C. Corros. Sci. 1963; 3: 139-143.

[16]Ennis P, Quadakkers W. Mechanisms of Steam Oxidation in High Strength Martensitic Steels. Int. J. Press. Vessels Pip. 2007; 84: 75-81.

[17]Karlsson A, Montgomery M. Survey of Oxidation in Steamside Conditions. VGB Kraftwerkstechnik, 1995; 75: 235-240.

[18]Saunders SR, Monterio M, Rizzo F. The Oxidation Behaviour of Metals and Alloys at High Temperatures in Atmospheres Containing Water Vapor; A Review. Prof. Mater. Sci. 2008; 53: 775-837.

[19]Otsuka N, Shida Y, Fujikawa H. Internal-External Transition for the Oxidation of Fe-Cr-Ni Austenitic Stainless Steels in Steam. Oxid. Met. 1988; 32(1/2): 13-45.

[20]Sabioni ACS, Huntz AM, Silva F, Jomard F. Diffusion of Iron in Cr_2O_3: Polycrystals and Thin Films. Mater. Sci. Eng. A. 2005; A392: 254-261.

[21]Sharp ZD. Determination of Oxygen Diffusion Rates in Magnetite From Natural Isotopic Variations. Geology. 1991; 19: 653-656.

[22]Young DJ. High Temperature Oxidation and Corrosion of Metals. Oxford: Elsevier, 2008.

[23]Atkinson A, Taylor RI. Diffusion of Fe in Fe_2O_3 Single Crystals. J. Phys. Chem. Solids. 1985; 46(4): 469-475.

[24]Wright IG, Tortorelli PF, Schutze M. Oxide Growth and Exfoliation on Alloys Exposed to Steam: EPRI; 2007 (report No. 1012666).

[25]Sabau AS, Shingledecker JP, Wright IG. Steam-side Oxide Scale Exfoliation Behaviour in Superheaters and Reheaters: Differences in the Behaviour of Alloys T22, T91 and TP347 Based on Computer Simulation Results, Proceedings of the 6th International Conference on Advances in Materials and Technology for Fossil Power Plants; 2010 Aug 31-Sep 3rd; Santa Fe, New Mexico.

List of figure captions:

Figure 1. Schematic diagram of the steam oxidation set up.

Figure 2. Secondary electron images of the inner pickled surface of TP347H FG exposed to air saturated steam at 650 °C for 100 hours (left) and 1000 hours (right).

Figure 3. Optical microscope image of a cross section through an unspalled region of TP347H FG exposed to air saturated steam for 1000 hours at 650 °C showing two outer iron rich oxides.

Figure 4. Back scattered electron cross section image through TP347H FG oxidised in air saturated steam for 1 x 100 hours at 650 °C (left) and the corresponding concentration profile measured using EDS and WDS showing the presence of Fe_2O_3 (40 at.% Fe, 60 at.% O) and Fe_3O_4 (42.9 at.% Fe, 57.1 at.% O) (right).

Figure 5. Back scattered electron cross section image of TP347H FG oxidised in air saturated steam for 1 x 300 hours at 650 °C (left) and the corresponding linescan profile measured along the yellow line using EDS, demonstrating the chromium rich oxide and the depletion seen beneath this layer (right).

Figure 6. BSE cross section image of TP347H FG oxidised in air saturated steam for 1 x 1000 hours at 650 °C (left) and the corresponding concentration profile measured using EDS and WDS showing the chromium rich oxide layer (right).

Figure 7. Depletion profiles measured using EDS of TP347H FG oxidised in steam for a total of 2000 hours at 650 °C where the second 1000 hours was carried out in a different environment. A greater depth of depletion was observed when oxidation was performed in air saturated steam.

Figure 8. Oxidation kinetics for both isothermal (triangles) and cyclic (circles) oxidation for TP347H FG exposed to air saturated steam at 650 °C.

Figure 9. Oxidation mechanism for long term thermal cycling of TP347H FG.

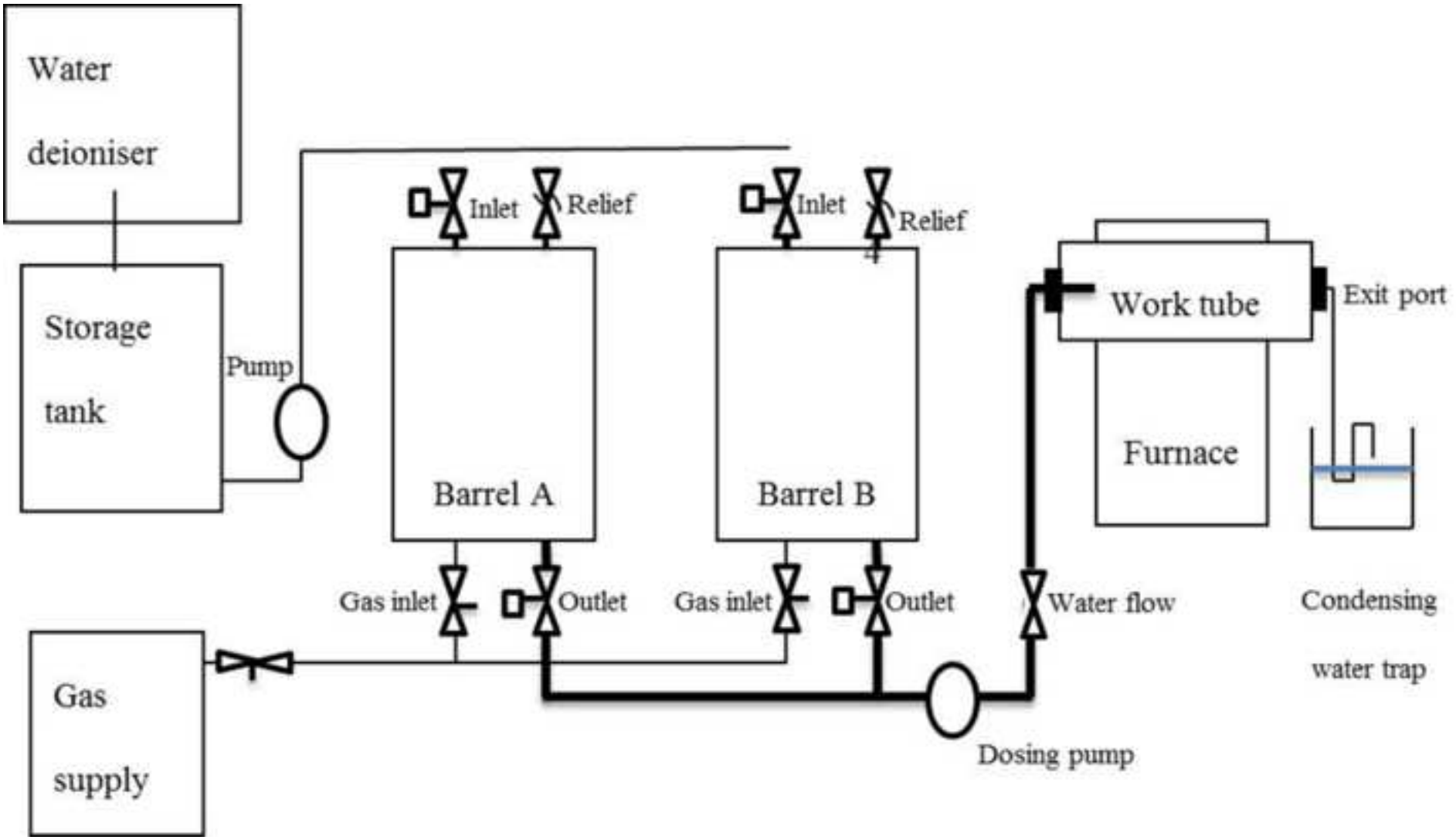

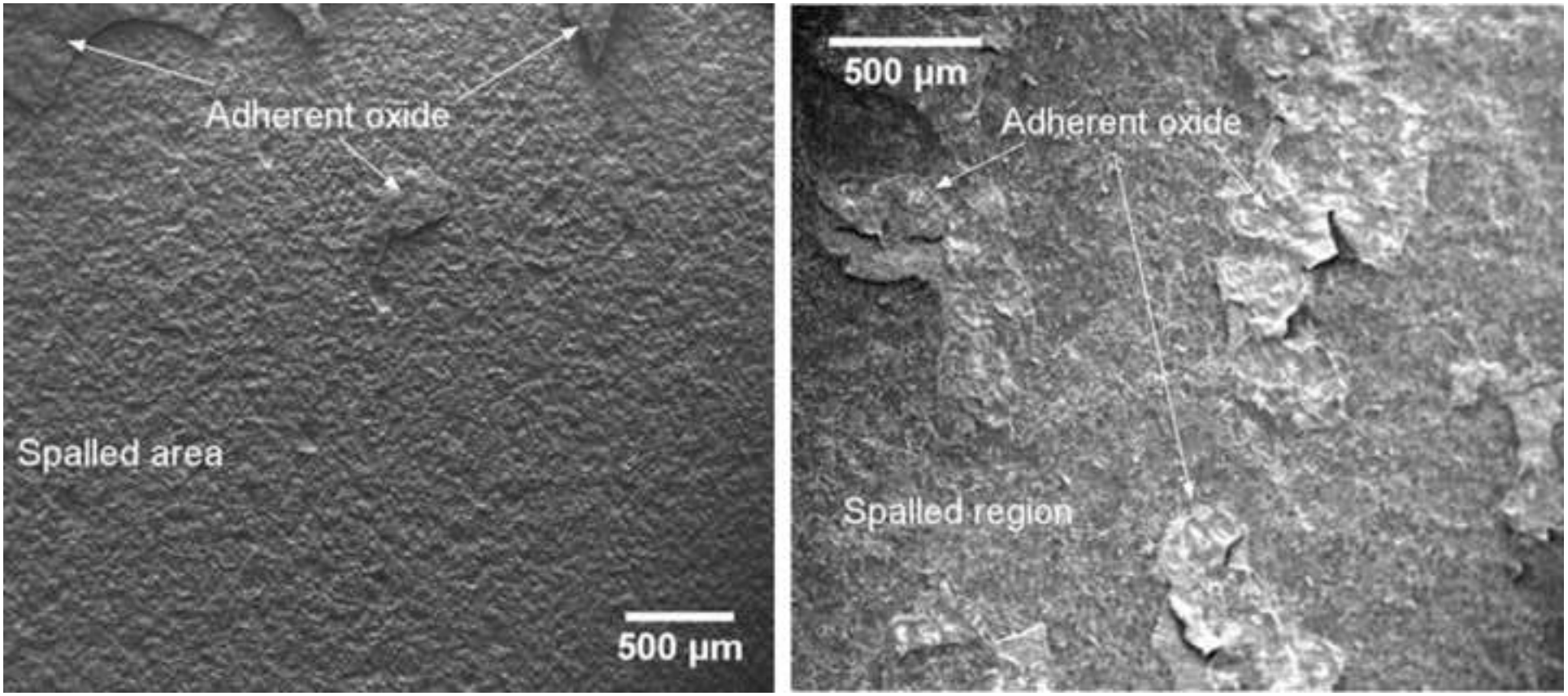

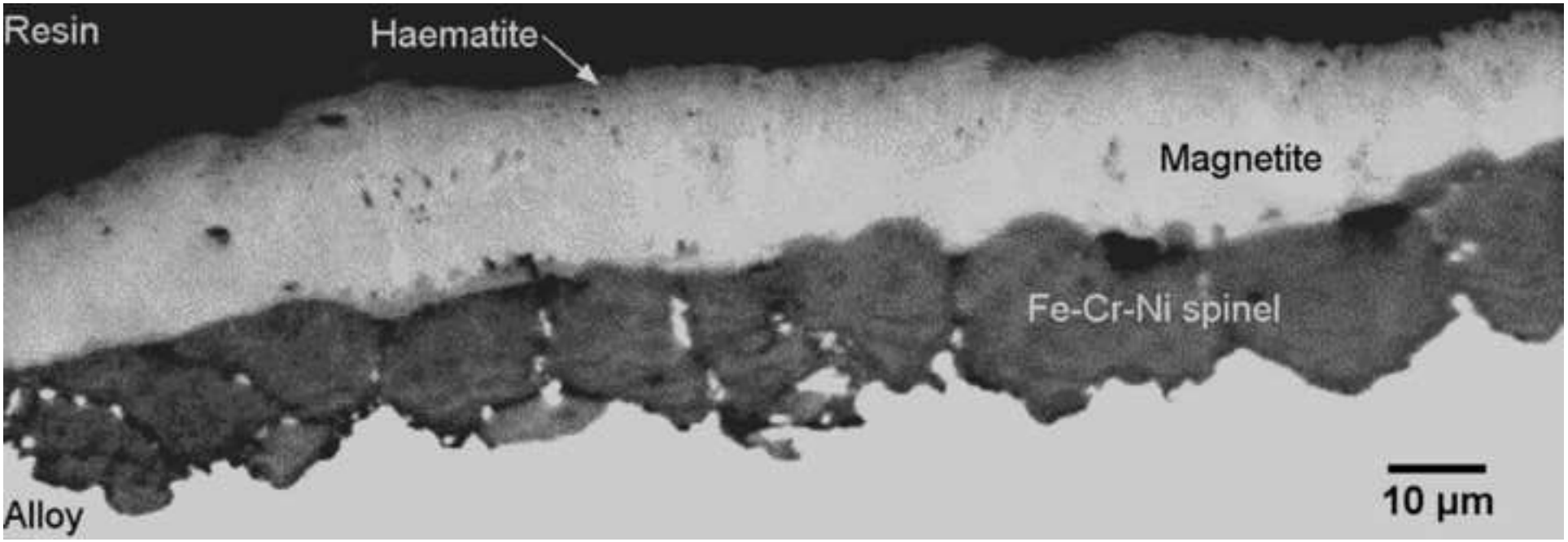

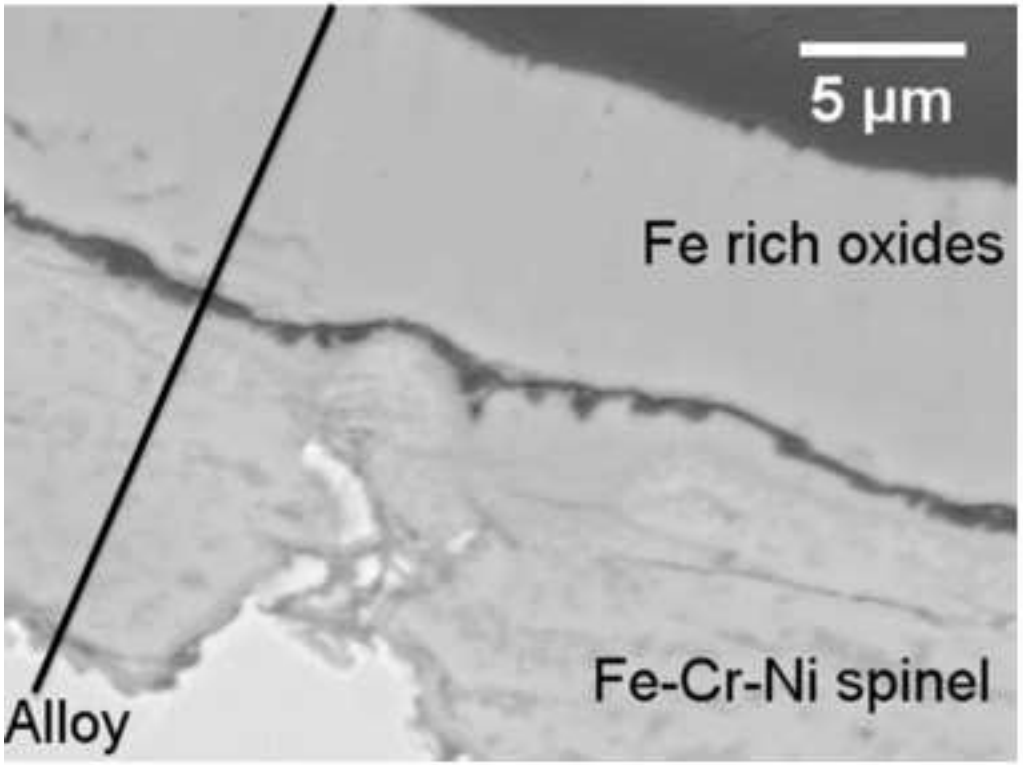

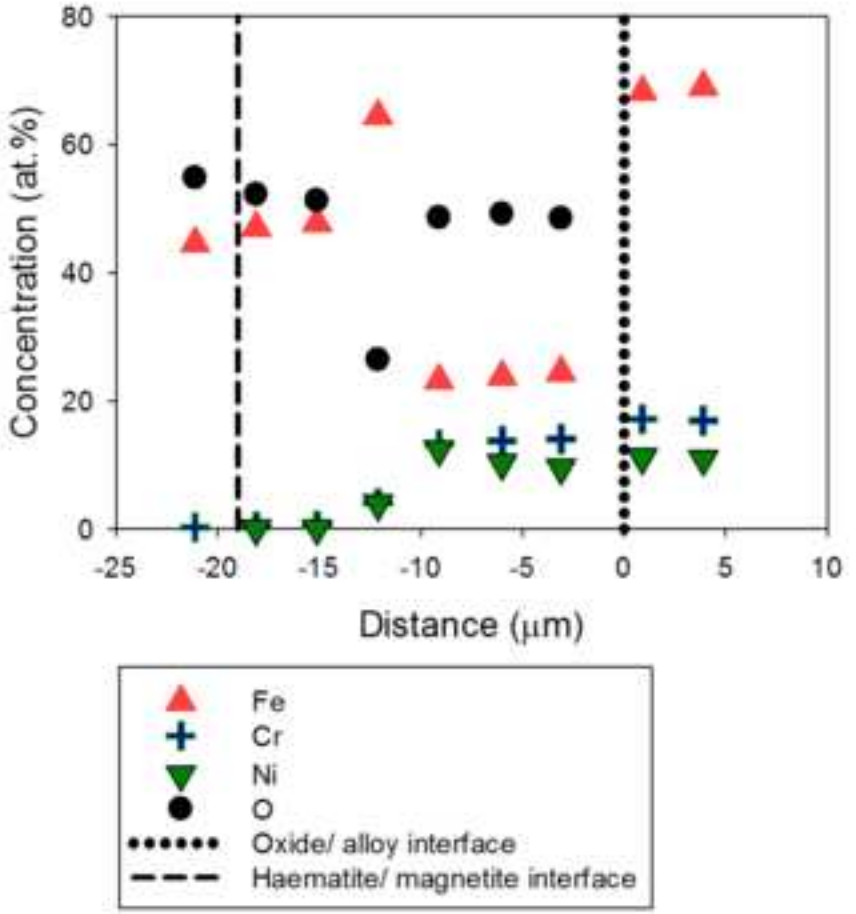

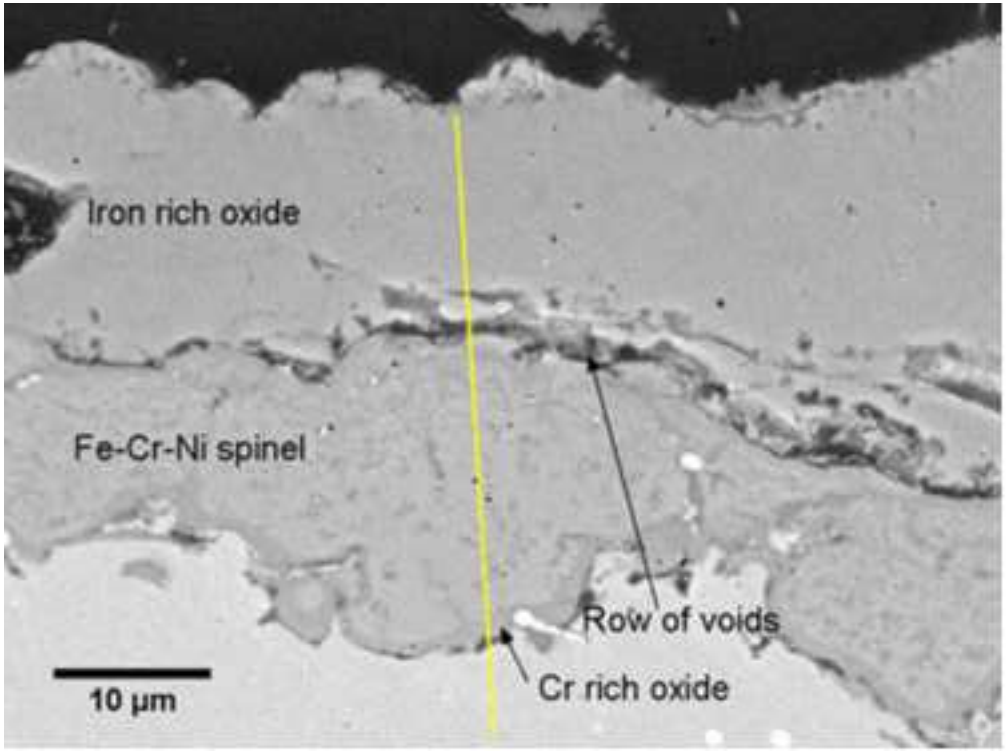

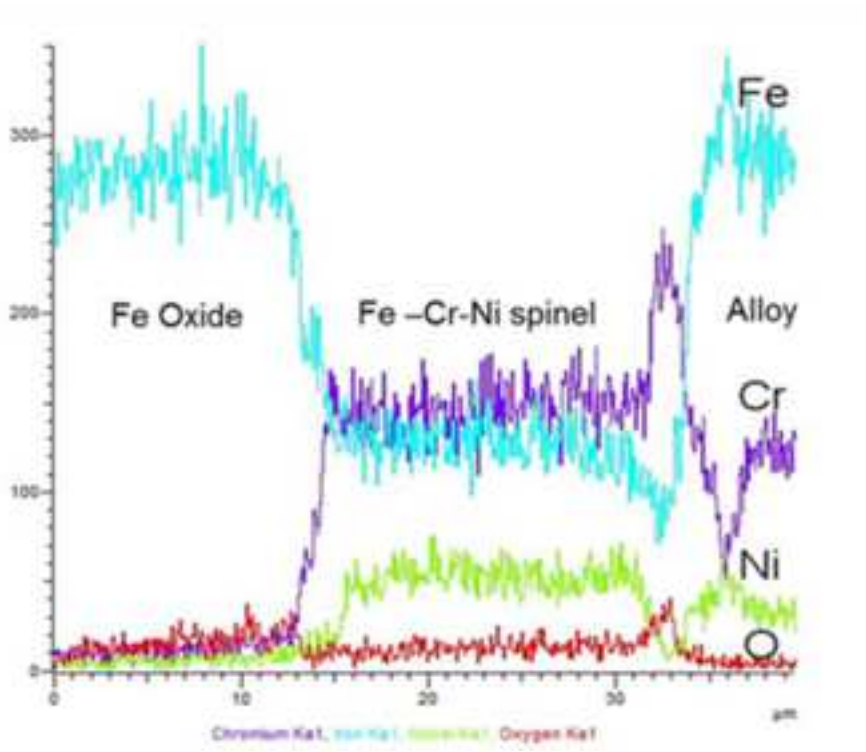

Colour figure (online version only)

Click here to download Colour figure (online version only) figure 5.tif